Resonant sound caused by flow past two plates in tandem in a duct

By S. A. T. STONEMAN, K. HOURIGAN,† A. N. STOKES‡
AND M. C. WELSH†

Department of Mechanical Engineering, University College Swansea, Singleton Park,
Swansea SA2 8PP, Wales

† Commonwealth Scientific and Industrial Research Organisation, Division of Construction
and Engineering, Highett, Victoria 3190, Australia

‡ Commonwealth Scientific and Industrial Research Organisation, Division of Mathematics
and Statistics, Clayton, Victoria 3168, Australia

Two plates placed in tandem in a duct flow shed vortices, which can excite and sustain an acoustic resonance associated with the duct. The sound can in turn 'feed back' and 'lock' the vortex shedding rate to the sound frequency. The experimental conditions under which loud resonant sound is sustained are described in this paper. The acoustic sources are predicted by combining a vortex model of the flow field with a finite-element solution of the sound field, and then using Howe's theory of aerodynamic sound to calculate the energy exchange between the flow and the sound field. Only in certain regions near the plates is substantial net energy exchange possible; the direction of energy transfer depends on the spacing of the plates. The region around the trailing edge of the upstream plate is found to be always a net acoustic source during resonance, while the region around the downstream plate is a net source or sink depending on the phase of the acoustic cycle at which vortices arrive there, which in turn depends on plate spacing and flow velocity. The net source region around the downstream plate is suppressed over a wide range of plate spacings by splitting this plate at midspan and rejoining it so that one half is offset in the flow direction by the distance a vortex travels in half a sound cycle.

1. Introduction

The phenomenon of flow induced acoustic resonance has been studied in detail since the 1940's when Batchelor & Townsend (1945) observed an acoustic resonance in the turning vanes of a wind tunnel at the University of Sydney. Two decades later, Parker (1966, 1967a) described the modal shapes of the acoustic resonances surrounding a vertical cascade of horizontal flat plates and defined them as the α, β, γ and δ modes, of which the β-mode was the simplest (Parker 1966). These resonances were generated by the flow and it was shown that their excitation did not require structural vibration (Parker 1969).

Away from the plates, the pressure amplitude distribution of the β-mode corresponds to an evanescent cross-mode of a duct. Near the plates, the impervious surfaces modify the modal shape to give a maximum acoustic pressure amplitude midway between the leading and trailing edges and midway between adjacent plates. Within each horizontal section bounded by adjacent plates the pressures are in phase; in adjacent sections they are of opposite phase. Consequently the acoustic

particle velocities oscillate, in phase, around the leading and trailing edges 90° in advance of the acoustic pressures above each plate.

Later more detailed studies by Cumpsty & Whitehead (1971), Archibald (1975), Welsh & Gibson (1979), Welsh, Stokes & Parker (1984), Welsh & Stokes (1986), Stokes & Welsh (1986) and others have examined the interaction between flow and flow-induced resonant sound with a single plate located in a duct. For this case the β-mode acoustic resonance was excited where the plates in a cascade were replaced by the duct walls. Away from the plate, the β-mode corresponded to an evanescent first cross-mode of the duct. The latter studies by Welsh *et al.* (1984), Welsh & Stokes (1986) and Stokes & Welsh (1986) described the mechanism by which the flow sustains an acoustic resonance. The explanation, given in terms of vorticity in the flow and the acoustic particle velocities, used Howe's (1984) theory of aerodynamic sound. A mathematical model of the acoustic sources described the energy transfer process between the flow and the sound fields.

Parker (1967b, 1968), Parker & Pryce (1974), Parker, Stoneman & Carr (1984), Parker & Stoneman (1984, 1985) and Stoneman (1984) have investigated acoustic resonances induced by flow in axisymmetric equipment such as axial flow compressors. They established that these resonances can excite significant structural vibration of the compressor blades at frequencies predicted neither by structural analysis of the system nor by the aeroelastic phenomena of flutter, propagating stall or surge. They also showed that the associated acoustic resonances existed over a wide range of Strouhal numbers and that the resonances could lead to a significant increase in the aerodynamic drag of the blading (Stoneman 1984). At the same time, the existence of flow-induced acoustic resonances in cross-flow heat exchangers was studied by other workers, including Zdravkovich & Nuttall (1974), Fitzpatrick & Donaldson (1977), Fitzpatrick (1985), Chen (1968, 1972), Chang & Yeh (1981), Byrne (1983), Cowell & Davenport (1984).

In both axial flow research compressors (in aero engine applications) and heat exchangers, the presence of acoustic resonances can have structurally deleterious effects and various methods have been proposed for their suppression. In the case of heat exchangers, Cowell & Davenport (1984) proposed a method for suppressing acoustic resonances using damping material in the walls. Chang & Yeh (1981) used a different approach and included one of the heat exchanger walls. This technique upset the matching that would otherwise exist between the acoustics of the space surrounding the tubes and the acoustic sources located in the flow. Chen (1968) also changed the acoustics of the space surrounding the tubes by locating baffles between them. Byrne (1983) refined this method by perforating the baffles with a series of holes to effectively increase the acoustic damping. Zdravkovich & Nuttall (1974) were able to suppress the resonances by eliminating the sources of acoustic vibration; they removed those tubes located near acoustic velocity antinodes in the second row of the tube bank.

Blevins (1985) recently published a study of the sound produced by vortex shedding from a single tube located in a duct, with a view to explaining the source of sound in heat exchangers. A study by Johnson & Loehrke (1984) of the sound generated by vortex shedding from two plates located in tandem in an open jet showed that the addition of the second plate had a significant effect on the sources of sound. When they used an upstream plate with a sharp trailing edge, a laminar wake formed at the flow velocities of interest. As the downstream plate was moved away from the upstream plate in flow direction, the frequency of the sound generated by the constant-velocity flow decreased gradually, then suddenly increased, then

decreased gradually again. This result was explained in terms of a 'feedback' mechanism akin to that described by Rockwell & Naudascher (1979) and Rockwell (1982) for flows past sharp edges. When the trailing edge of the upstream plate was blunt and a turbulent wake was generated, the characteristics of the sound field generated by the vortex shedding from the plates were very different from the laminar case. At a constant flow velocity the amplitude of the sound, of constant frequency, varied periodically with changes in plate spacing. Johnson & Loehrke (1984) concluded that in this latter case there was no feedback and that the sound was generated by multiple sound sources which alternately cancelled and reinforced each other as the plate spacing increased.

The study reported in this paper examines the excitation process of the simplest transverse resonant duct acoustic mode generated by the high-Reynolds-number separated flow past two plates located in tandem in a rigid walled duct. The aim is to explain the multiple sound sources, referred to by Johnson & Loehrke (1984), and to examine in detail how these sources interact with each other. It should also be noted that a flow-induced acoustic resonance typically occurs within certain ranges of operating conditions. The effect of most of the remedies mentioned above is to change those ranges so that they do not coincide with normal operation. They are generally impractical in variable-speed situations, as for example in the axial flow compressors used in jet engines, where the operating schedule can be from 0 to 100 % design speed. It would be better, if possible, to identify the fairly restricted regions in the flow where net energy could be transferred from the flow to the sound field (acoustic sources) and then prevent this transfer. A second aim of the paper is to provide a simple example of how the understanding of the fundamental mechanism of this energy transfer can be applied to alter a particular source so that it does not contribute a net supply of acoustic energy to sustain the resonance. Here, this is achieved through changing the geometry of the downstream plate by offsetting it at midspan. It is likely that a general method for suppressing resonances in multibladed or tubed equipment will come from an approach that involves a similar understanding of the fundamental mechanism of the energy transfer between the sound and the flow fields.

Only the case where the vortex shedding and the resonant acoustic frequencies are 'locked' together will be modelled; future publications will present results of the case where the two frequencies are not locked. In the present locked case, the resonant sound field feeds back onto the separating shear layers and causes two vortices, one of each sign, to commence growing during each acoustic cycle. The excitation mechanism of flow-induced acoustic resonance is modelled mathematically in terms of the vorticity and the acoustic particle velocities. A surface vorticity method is used to specify the boundary conditions while a discrete vorticity method is used to predict the separated flows. A finite-element solution of the Helmholtz equation is used to predict the acoustic properties of the space surrounding the plates. These predictions are then coupled to calculate the acoustic power generated by the vortices passing through the resonant sound field using Howe's (1984) theory of aerodynamic sound. Thus, the regions in the flow where energy is transferred to the sound field and also the phase relationship between the acoustic field and the flow necessary for this to occur are identified. It is shown that the acoustic response of the duct system corresponds to the predicted acoustic energy generated by the flow around the plates as the plate spacing increases.

The paper is set out in the following way. Section 2 describes the experimental equipment while §3 sets out the theory and methods used to calculate the sound field,

the unsteady flow field, and then the interaction between them. To illustrate some unfamiliar concepts arising in the interaction, an example is given of a vortex of infinitesimal strength passing a single plate. A case closer to reality is examined in §4.

Section 4 covers the results of both experiment and calculation. First the results of the analysis of the acoustic modes are given, and then the experimental observations of circumstances in which they were excited are presented. These circumstances included different flow velocities and different arrangements of plates. There are three subsections covering, respectively, just one straight plate in the duct, two straight plates of similar shape, and finally two plates where the downstream plate had a more complicated shape designed to be an ineffective source according to the theory described. Finally, the results of combining mathematical models of the unsteady flow with the calculated sound field are described for the single plate and the plates in tandem.

Section 5 develops aspects of the general theory from §3 to decide which aspects of the flow are causing the observed patterns of resonance, and how they can be countered. In particular, reasons are given for the chosen design of the 'offset' plate used in the third series of experiments, and some other ways of achieving the same effect are suggested. Section 6 sets out the conclusions of the study.

2. Experimental apparatus and procedure

The acoustic resonances generated by the flow around the plates were investigated in an open-circuit wind tunnel where the air was drawn through the working section by an axial flow fan. This tunnel was specifically designed for the study of flow-induced acoustic resonance and is shown schematically in figures 1 and 2. The flow in the working section outside the boundary layers was uniform within 1 % and the longitudinal turbulence level was 0.04 % between spectral limits of 2–150 Hz.

The working section was 2.88 m and 244 mm square internally. The walls were mostly constructed from 12 mm thick aluminium and 47 mm thick methyl methacrylate (acrylic). Near the plates the walls were constructed from 25 mm thick methyl methacrylate and 6 mm thick glass fixed in an aluminium frame. The aluminium frame was bolted firmly to the duct walls to reduce the radiation of acoustic energy through the wall and increase the amplitude of the acoustic field around the plates. All the plates used in this investigation were located on the duct centreline with the upstream plate fixed and the downstream plate able to be moved axially from the trailing edge of the upstream plate to a position 200 mm downstream (figure 2). Each plate had a semicircular leading and trailing edge. The upstream plate had a chord of 66.7 mm and a thickness of 8 mm while the cross-section of the downstream plate was 40 mm by 5 mm. Two different downstream plates were used in two series of experiments. Each had the same cross-section, but while one was uniform in the spanwise direction, the other had been cut at midspan, and rejoined with an offset, so that one half was displaced 12 mm relative to the other in the flow direction (figure 1). An additional test was carried out for comparison with just the upstream plate (66.7 × 8 mm) installed.

Two microphones were used to record the acoustic pressure field in the duct (figure 2). One microphone was mounted 310 mm upstream of the upstream plate and flush with the inner surface of the working section. Its output was displayed directly onto a cathode ray oscilloscope and was used to monitor the phase of the acoustic field relative to the position of the vortices observed while using a strobe light or taking
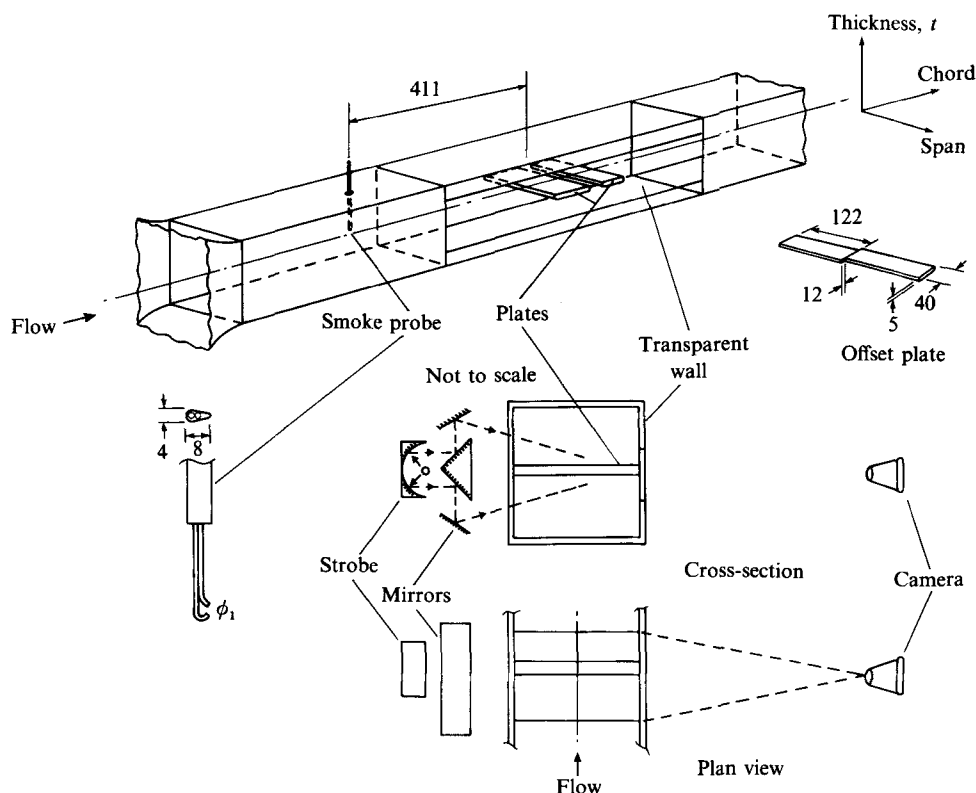
FIGURE 1. Schematic of wind tunnel working section and test equipment.
Dimensions are in mm.

photographs. A probe microphone was located 40 mm below the inner surface of the top wall and 97 mm upstream of the upstream plate; the outside diameter of the probe, which was shaped like a Pitot-static probe (figure 2), was 1 mm. An elliptical nose cone was fitted to the probe with the sensing hole positioned 4 mm downstream of the leading edge (figure 2). Since the sensing hole was outside the boundary layer on the top wall it was only slightly influenced by the aerodynamic pressure fluctuations due to the boundary layer. During flow-induced acoustic resonance, the sound pressure level (SPL) in the frequency range of interest (672–694 Hz) rose to approximately 150 dB (re 20 µPa). The background noise levels inside the duct without flow, in the same frequency range, were typically 40 dB. The probe microphone was calibrated after steel wool was inserted into the tube to ensure a flat frequency response over the desired frequency range (672–694 Hz).

A hot-wire sensor was placed 15 mm above the centreline of the duct and 29.3 mm downstream of the trailing edge of the upstream plate to record the velocity perturbations due to vortex shedding from the upstream plate (figure 2). This location of the hot wire reduced its sensitivity to the acoustic particle velocities which were approximately orthogonal to the flow velocity at this location.

Both the probe microphone and the hot-wire signals were digitized at 1600 Hz after band passing between 100 and 800 Hz. The frequencies of the spectral peaks, corresponding to the sound and the vortex shedding, were obtained after averaging ten spectra, which were each determined using a ninth-order FFT giving a bin width
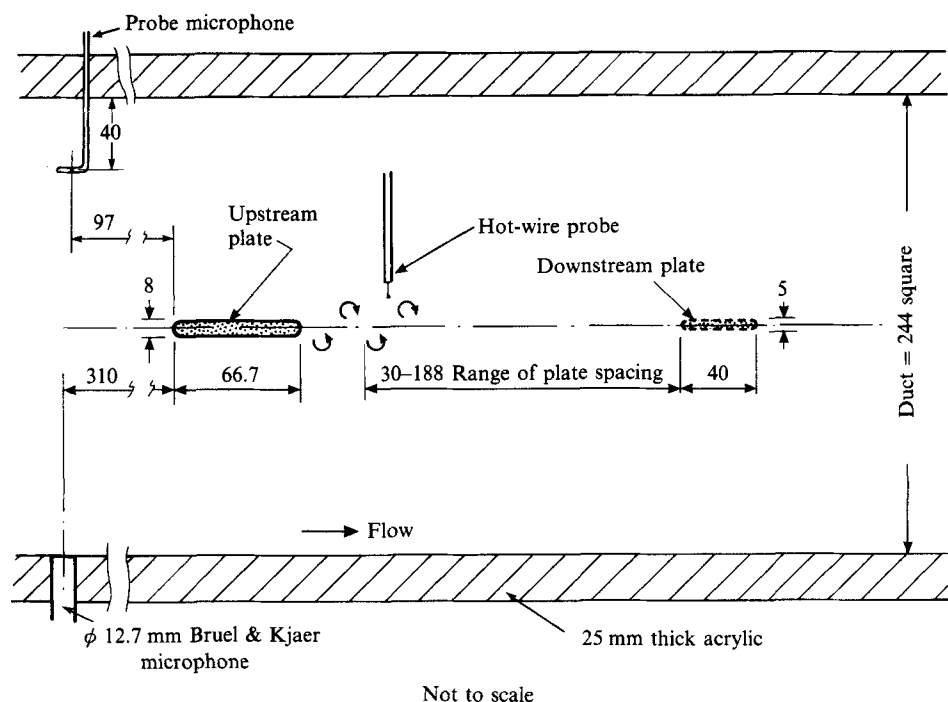
FIGURE 2. Close-up of sensors near the plates. Dimensions in mm.

of 3.125 Hz. The SPL's were determined from the amplitude of the spectral peak recorded by the probe microphone. These spectral peaks occurred at frequencies within 19 Hz of the resonant frequency at the maximum SPL recorded for each plate configuration with locked vortex shedding. For all of the plate configurations tested, the relevant acoustic spectral peaks occurred between 672 and 694 Hz. The vortex shedding frequencies were determined from the spectral peaks in the averaged spectra of the hot-wire signals.

The photograph (figure 11) showing the flows described in this paper was obtained by superimposing twenty exposures taken at the same phase angle in the acoustic cycle. A variable time-delay circuit ensured that the high-speed flash unit operated when the acoustic velocities were a maximum in the upwards direction. The exposures were recorded over a five minute period.

All of the tests were carried out at Reynolds numbers, based on upstream flow velocity and the thickness of the upstream plate, ranging from 1×10^4 to 2×10^4 at ambient conditions in the laboratory (approximately 17 °C and 101 kPa).

3. Mathematical models of the acoustic field and its interaction with the flow

3.1. *The acoustic field*

The acoustic modes for a duct with two or more plates in tandem on the midline of the duct are similar to those with just one plate (Parker 1967 *a*), and are obtained by

the same means. In the flows of interest here, the Mach number is small and the acoustic pressure p satisfies the wave equation

$$\frac{\partial^2 p}{\partial \tau^2} = c^2 \nabla^2 p, \tag{3.1}$$

where c denotes the velocity of sound and τ is time. From a standing-wave solution may be extracted the time-independent amplitude function ϕ:

$$p = \phi e^{2 i \pi f \tau}, \tag{3.2}$$

where f is the frequency of the mode. Then ϕ satisfies the Helmholtz equation

$$\nabla^2 \phi + (2\pi f/c)^2 \phi = 0. \tag{3.3}$$

The boundary conditions for the modes antisymmetric about the midline are

$$\boldsymbol{n} \cdot \nabla \phi = 0, \tag{3.4}$$

$$\phi = 0, \tag{3.5}$$

where (3.4) applies to rigid surfaces ($\boldsymbol{n}$ = surface normal vector) and (3.5) applies on the duct midline (except where plates are present).

This elliptic boundary-value problem was solved by the finite-element method using triangular elements and piecewise linear shape functions. The resulting system of linear equations for the values of ϕ at the nodes was symmetric and banded. The resonant mode frequencies are the eigenvalues of the matrix of coefficients and the corresponding eigenvectors give the nodal pressure amplitudes. The smallest eigenvalue gives the simplest solutions, for which ϕ has the same sign in the solution region (one half of the duct). For the case of a single plate, this is the Parker β-mode (Parker 1966, 1967 a).

If $\boldsymbol{A}$ is the symmetric banded matrix of coefficients, then the eigenvalue λ is found by solving

$$\det(\boldsymbol{A}-\lambda\boldsymbol{I}) = 0 \tag{3.6}$$

by the secant method. This is essentially Newton's method, except that the derivative is estimated from the difference of successive approximations. The determinant is calculated by LU factorization of the matrix, i.e. expressing it as the product of an upper triangular and a lower triangular matrix. If the lower triangular factor L is normalized to have unit diagonal, then the determinant is just the product of the diagonal terms of the upper triangular factor U. $\boldsymbol{A}$ is positive definite, so for the least eigenvalue the diagonal of U will have one zero element, with the rest positive. For the next eigenvalue, there will be one negative element, and so on. Although this method is not the quickest for obtaining the least eigenvalue, it allows direct calculation of higher-order modes with an indicator of which mode is found.

3.2. *The flow field*

The flow is modelled by a two-dimensional inviscid incompressible flow, irrotational everywhere except at the centres of elemental vortices. The assumption of two-dimensionality is justified in the present model because the presence of a loud resonant two-dimensional transverse mode sound field is observed to force the vortex shedding and subsequent large-scale structures to be two-dimensional (Parker 1969). The shedding of vorticity is modelled by the creation of the elemental vortices, which

are convected under the influence of other vortices and the irrotational flow. Because of the assumptions about the flow, a potential may be defined that is multivalued but which satisfies the Laplace equation on each of its branches, except at vortex centres.

In the technique used by Lewis (1981), the surface vorticity method is used to predict the vorticity distribution along the body surfaces. This method has sometimes been used as an alternative to the surface source panel method; the surface vorticity method has the advantage of representing, even in potential flow, a first approximation to the natural boundary layer through satisfying the surface no-slip condition. The shedding of vorticity into the flow in the present case of flow around curved boundaries does not involve the Kutta condition, which strictly interpreted is applied to remove singularities in pressure and velocity (Crighton 1981). Interpreted more loosely for flows near surfaces without sharp corners, the Kutta condition could involve the introduction of a vortex into the flow to produce a zero velocity at a prescribed shedding point on the body surface. However, in the method adopted by Lewis (1981), vortex segments are placed along the entire body surface to satisfy the no-slip condition at the centre of each segment, and vortices are directed into the flow at designated shedding points with circulations determined by the local rate of vorticity generation.

In the surface vorticity method, the distribution of vorticity along the surface must meet the requirement of zero velocity on the inside of the sheet and ensure that the contour is a streamline. The linear vorticity density $\gamma(s)$ at distance s along the surface of a two-dimensional body in irrotational flow is provided by the solution to the Fredholm equation:

$$\oint \gamma(s_n) K(s_n, s_m) \, \mathrm{d}s_n - \tfrac{1}{2}\gamma(s_m) = -U_x \left(\frac{\mathrm{d}x_m}{\mathrm{d}s}\right) - U_y \left(\frac{\mathrm{d}y_m}{\mathrm{d}s}\right). \tag{3.7}$$

Here, the local components of the velocity of the irrotational flow in the x- and y-directions are U_x and U_y, respectively. The coupling coefficient $K(s_n, s_m)$ has the value of the surface tangential velocity at s_m induced by a vortex of unit circulation at s_n.

Discretizing the body profile into M segments of length Δs_n, $(n = 1, M)$, produces a set of linear equations:

$$\sum_{n=1}^{M} \Delta s_n \gamma(s_n) K(s_n, s_m) - \tfrac{1}{2}\gamma(s_m)$$

$$= -(v_x + v_{x,\mathrm{s}}) \left(\frac{\mathrm{d}x_m}{\mathrm{d}s}\right) - (v_y + v_{y,\mathrm{s}}) \left(\frac{\mathrm{d}y_m}{\mathrm{d}s}\right) - \sum_{n=1}^{N_v} \Gamma_n T(n, s_m) \quad (m = 1, M), \tag{3.8}$$

where the last term in (3.8) gives the contribution to the velocity field at the surface due to N_v free vortices of circulation Γ in the flow. The coupling coefficient $T(n, s_m)$ has the value of the surface velocity at s_m due to a vortex of unit circulation at the position of the nth free vortex. Here, the velocity of the irrotational flow has been separated into steady (v_x, v_y) and unsteady acoustic $(v_{x,\mathrm{s}}, v_{y,\mathrm{s}})$ components; these acoustic components of the velocity are provided by the finite-element solution described in §3.1. Because the wavelength of the acoustic mode is long compared with the dimensions of the vortex structures, locally the assumption of incompressibility is not violated.

The solution of (3.8) gives the surface vorticity density at the pivotal points on the surface of the body, which are taken to be the centre of each discrete element. In the present code, each body profile was discretized into 148 ($= M$) segments. The lengths of the individual segments were set according to a sinusoidal compression factor along each edge of a plate, which concentrates more segments near the corners where the highest velocity gradients and curvature are found.

Vorticity is generated at the body surface owing to tangential pressure gradients (Lewis 1981; Morton 1984) and moves away from the boundary through viscous diffusion. For an inviscid fluid, the boundary-layer thickness is infinitesimal and is represented by the surface vorticity elements. The velocity on the outer edge of the surface element is equal to the surface vorticity density. Although the model is capable of handling more points of flow separation, in the present model the vorticity shedding is assumed to be confined to the trailing edge of the upstream body; the experimental observations indicate that this is the major region in which the flow structures develop and restricting the number of separation points leads to computational economy. The separating shear layer at a trailing edge is represented by discrete elemental vortices. The circulation of a nascent elemental vortex is calculated using the local surface vorticity density and convection velocity at the centre of the surface segments immediately preceding the rounded trailing edge. The elemental vortices are initially directed at an angle of 45° to the body surface in order that a well-defined shear layer is represented. Lewis (1981) found that this numerical artifice produced satisfactory results for the shedding from curved surfaces; the exact angle is not critical but allows simulation of viscous effects which initially diffuse vorticity away from the surface and permits roll-up of the shear layer.

Interaction between the point vortices is 'smoothed' by assuming a Rankine vortex velocity field within $0.05t$ of their centres, where t is the upstream plate thickness. The formation of the large-scale structures is found to be insensitive to the exact smoothing value used (Kiya, Sasaki & Arie, 1982). The vortices are advected using a second-order Eulerian scheme; a time-step of $0.02(t/v_\infty)$ is used, where v_∞ is the upstream-infinity flow velocity. New elemental vortices are released every fourth time-step, which is a sufficiently short period to allow a reasonably smooth approximation to the separating shear layer. The amplitude of the acoustic particle velocity at the centre of the trailing edge of the upstream plate is set to $0.2v_\infty$, in line with its estimation from the measured sound pressure levels; the shedding of the large-scale vortices does not appear, from the observations, to be sensitive to the precise value of the amplitude for loud resonances. At distances beyond $20t$ downstream of the first plate, the elemental vortices were gradually merged to economize the calculations, which were performed on a Cyber 205 computer.

3.3. *The sound-flow interaction*

Howe (1984) showed that when an acoustic oscillation occurs in an inviscid, isentropic but rotational flow, then an acoustic power P is generated in a volume V, which is given by

$$P = -\rho_0 \int \boldsymbol{\omega} \cdot (\boldsymbol{v} \times \boldsymbol{u}) \, \mathrm{d}V, \tag{3.9}$$

where $\boldsymbol{v}$ is the total fluid velocity, including that induced by transient vorticity, $\boldsymbol{\omega} = \nabla \times \boldsymbol{v}$ is the vorticity, $\boldsymbol{u}$ is the acoustic particle velocity and ρ_0 is the density of the fluid.

When the vorticity is 'compact', that is when the vorticity extends over a region
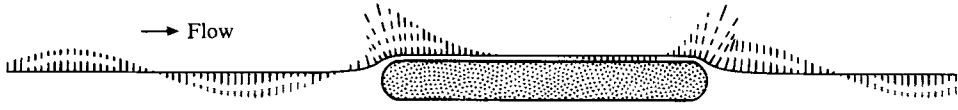
FIGURE 3. Path of a single vortex of infinitesimal circulation passing a plate (——);
instantaneous acoustic power P proportional to the length of the line segment (- - - -).

that is small relative to the acoustic wavelength, then the acoustic power/unit length
of vortex tube generated by a vortex reduces to

$$P = -\rho_0 \Gamma \boldsymbol{k} \cdot (\boldsymbol{v} \times \boldsymbol{u}), \tag{3.10}$$

where Γ is the circulation of the vortex and $\boldsymbol{k}$ is the unit vector normal to the plane
of the flow.

This acoustic power is oscillatory over time because of the oscillation of the
acoustic particle velocity; it is therefore useful to factorize P to separate this
oscillatory term. First $\boldsymbol{u}$ is factorized:

$$\boldsymbol{u} = \boldsymbol{u}_0 \sin(2\pi f\tau + h), \tag{3.11}$$

where $\boldsymbol{u}_0$ is the steady amplitude of the sound field, f is its frequency and h is a phase
constant. Then

$$P = Q \sin(2\pi f\tau + h), \tag{3.12}$$

where $Q = -\rho_0 \Gamma |\boldsymbol{v}| |\boldsymbol{u}_0| \sin \alpha$ and α is the angle between $\boldsymbol{v}$ and $\boldsymbol{u}_0$.

For the present flow and sound field, the factors of Q do not vary with time at a
fixed location, but do vary with location. If the vortex motion is steady in a uniform
sound field, then there is no change at all in Q; P oscillates sinusoidally and the net
energy transferred per acoustic cycle, which is the time integral of P, is zero. Only
when either the sound field or flow varies is there net acoustic energy gained or
lost.

To illustrate the requirement for a change in Q to produce acoustic energy, figure
3 shows the path of a vortex of vanishingly small but constant circulation passing a
plate of the shape of the downstream plate used in the present experiments. There
is assumed to be an acoustic field which in the far field is a uniform vertical
oscillation. Plotted orthogonal to the path of the vortex are line segments whose
lengths represent the value of P when the vortex is at the intersection of the line
segments with the path. The uniform oscillation attained at a distance from the plate
is apparent but the form of this plot is sensitive to the phase h. That is, the value of
P is very dependent on the direction and amplitude of the acoustic particle velocities
when the vortex passes a given point.

Q is plotted in figure 4 as a function of time, together with the factors of Q. In the
particular circumstances assumed, that is steady vortex velocity and circulation and
time-independent acoustic particle velocity magnitudes, the dominant variation of Q
is due to the spatial variation of the magnitude of the acoustic particle velocity. This
velocity magnitude increases as the vortex passes the ends of the plate and becomes
small midway between the ends of the plate; P and Q behave similarly. At the phase
assumed, the reduction in Q near the midplate happens when the vortex would
otherwise be involved in the absorption of energy from the acoustic field; summed
over time, this gives a net gain of energy to the sound field. This gain is reinforced
at the ends of the plate, where a peak in Q occurs when the vortex is involved in the
transfer of energy to the sound. Had the vortex arrived half a sound cycle later, these
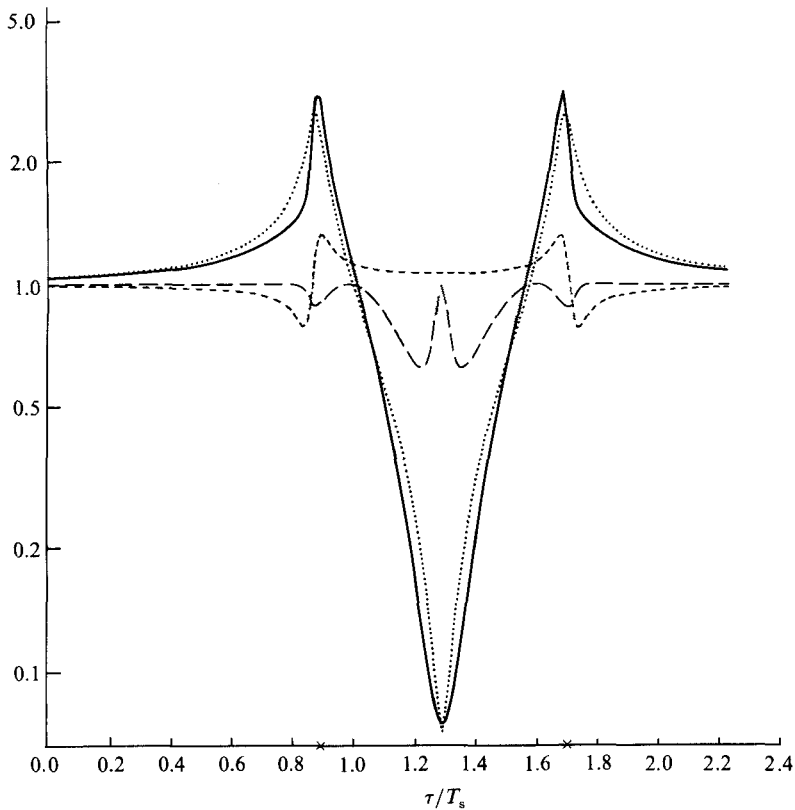
FIGURE 4. Variation with time of the normalized components of the modified expression or acoustic power generated by a vortex following the trajectory of the vortex shown in figure 3: ———, $Q(\tau)$; ······, $|\boldsymbol{u}_0|$; -----, $|\boldsymbol{v}|$; ———, $\sin \alpha$; ×, instants when the vortex passes the leading and trailing edges of the plate. Component values are normalized to their upstream infinity values and plotted on a logarithmic scale. T_s is the period of an acoustic cycle.

effects would have been reversed and a net absorption of energy from the sound field would occur.

The total energy transferred from the vortex to the sound field is the time integral of P. Although the oscillations shown in figure 3 make this integral impossible to calculate directly, it can be conveniently integrated by parts since the time derivative of Q, $Q'(\tau)$, rapidly approaches zero as the vortex recedes from the plate. Integration by parts is based on the formula

$$W - P = \frac{\mathrm{d}}{\mathrm{d}\tau}\left[\frac{Q(\tau)}{2\pi f}\cos\left(2\pi f\tau + h\right)\right], \qquad (3.13)$$

where

$$W = \frac{Q'(\tau)}{2\pi f}\cos\left(2\pi f\tau + h\right). \qquad (3.14)$$

On integration over time, from 0 to ∞, the right-hand side of (3.13) gives a zero result, because the vortex circulation is initially zero and $Q(\tau)$ eventually reduces to zero along with the acoustic field. The result is that

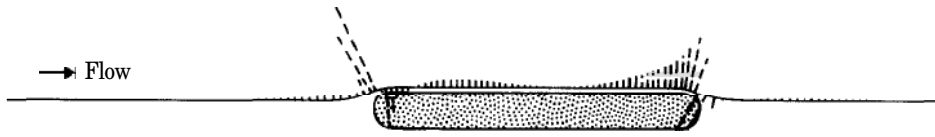$$\int_0^\infty P\,\mathrm{d}\tau = \int_0^\infty W\,\mathrm{d}\tau. \qquad (3.15)$$

FIGURE 5. Path of a single vortex of infinitesimal circulation passing a plate (———); the modified integrand W(τ), shown for the same vortex trajectory as figure 3, proportional to the length of the line segment (– – – –).
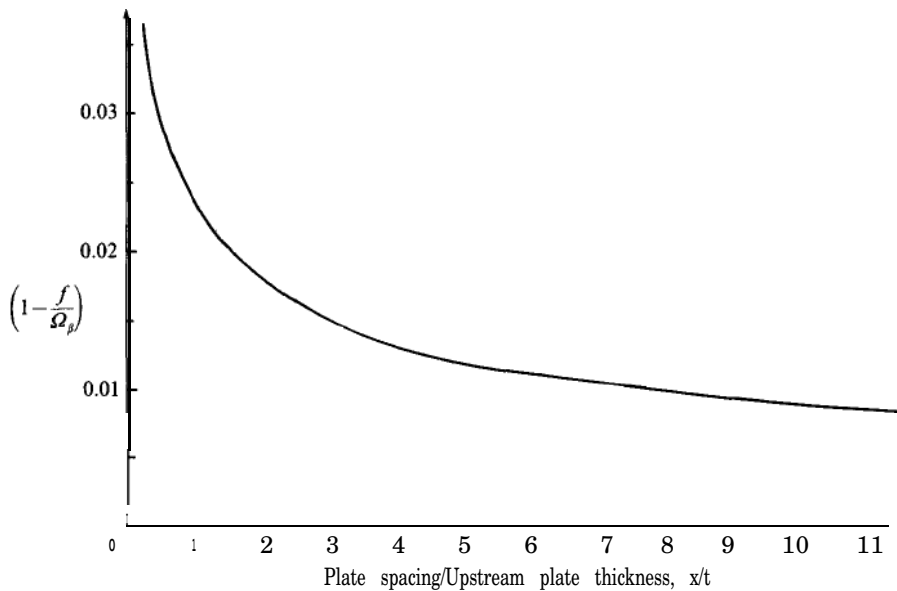

FIGURE 6. Variation of resonant sound frequency with plate spacing: $\Omega_\beta = \beta$-mode resonant frequency for upstream plate alone ; f = resonant frequency for both straight plates installed in tandem, separated by distance x; chord of upstream plate = 66.7 mm; chord of downstream plate = 40 mm; thickness of upstream plate t = 8 mm; thickness of downstream plate = 5 mm.

W is plotted in figure 5 in a manner analogous to that described for figure 3. W is seen to be almost zero everywhere except near the ends of the plate. This facilitates numerical evaluation of the integral and also makes W a useful aid to physical interpretation. In particular, the peaks in W can be used to define acoustic sources or sinks in the flow. Any modification to the flow that is intended to change the total acoustic energy extracted from the flow must be undertaken in the region where the magnitude of W is large.

The quantities P and W are proportional to vortex circulation, and since the scale of the plots in figures 3 and 5 is arbitrary, they would apply equally to vortices of finite circulation. The only difference is that such vortices would follow a somewhat different path; they are, in effect, influenced by their images beyond the solid boundaries.

4. Results

4.1. Simplest resonant acoustic mode surrounding two plates in a duct

The simplest resonant transverse duct acoustic mode with one plate located on the duct centreline is the P-mode as defined by Parker (1966, 1967a). When a
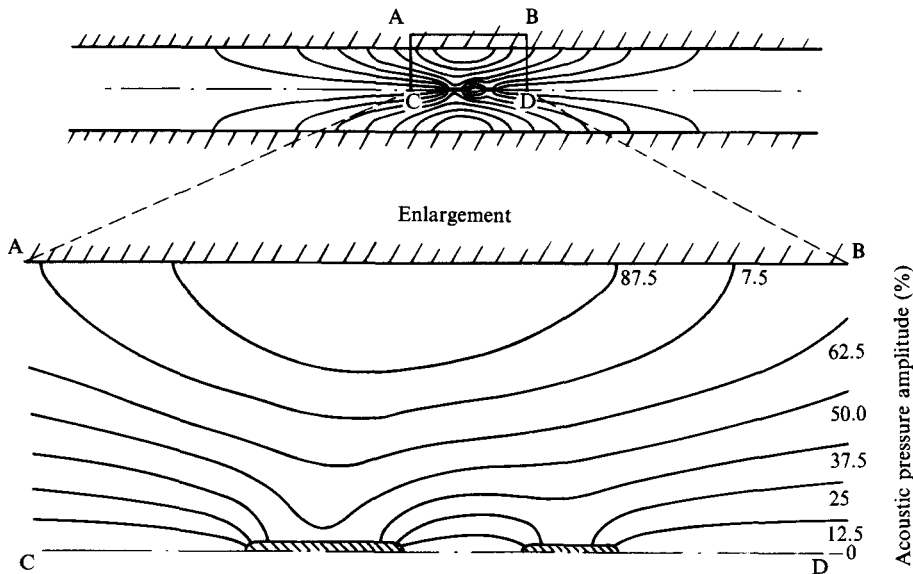
FIGURE 7. Contours of acoustic pressure amplitude for the simplest resonant acoustic mode for two straight plates located in tandem at a spacing of $x/t = 6.25$ (50 mm) on the centreline of a hard-walled duct; contour valves are expressed as the percentage of the maximum acoustic pressure on the duct wall above and below the upstream plate.

downstream plate is located in the same central plane, that is in tandem with the upstream plate, a similar resonant mode can exist but at a lower frequency. The resonant frequency f varies with the spacing x of the plates, but is always less than the β-mode resonant frequency Ω_β for the upstream plate installed alone. In figure 6, this variation is shown using the normalized distance x/t and the frequency ratio f/Ω_β. The frequencies were calculated using the finite-element method described in §3.1.

The geometry of the plates is described in §2. When they are at zero spacing, the resonant frequency f is significantly lower than Ω_β. This is to be expected since the resonant frequency is then that of a single plate of the combined chords, and Parker (1967 a) showed that the β-mode resonant frequency reduces as the chord of the plate increases. As the plate spacing increases, the resonant frequency increases and asymptotes towards the β-mode frequency of the upstream plate alone. For the non-dimensional plate spacings of $x/t = 3.75$–23.5 (30–188 mm) described in this paper, the calculated resonant frequency changes by approximately 5 Hz.

Figure 7 shows the pressure amplitude contours corresponding to the resonant mode that may exist when the two plates are spaced at $x/t = 6.25$ (50 mm). As with the β-mode for a single plate, when the acoustic pressures above the plates at any given instant are greater than the mean, those below the plates are less than the mean. When the plates are close together, there is a single pressure maximum on the wall above the larger plate. At greater separation, there may be a second local maximum on the wall above the smaller plate. Because the mode frequency is below cut-on for the first cross-mode of the duct without plates installed (703 Hz), there is exponential decay in the amplitudes of the acoustic variables in both the upstream and the downstream directions away from the plates.

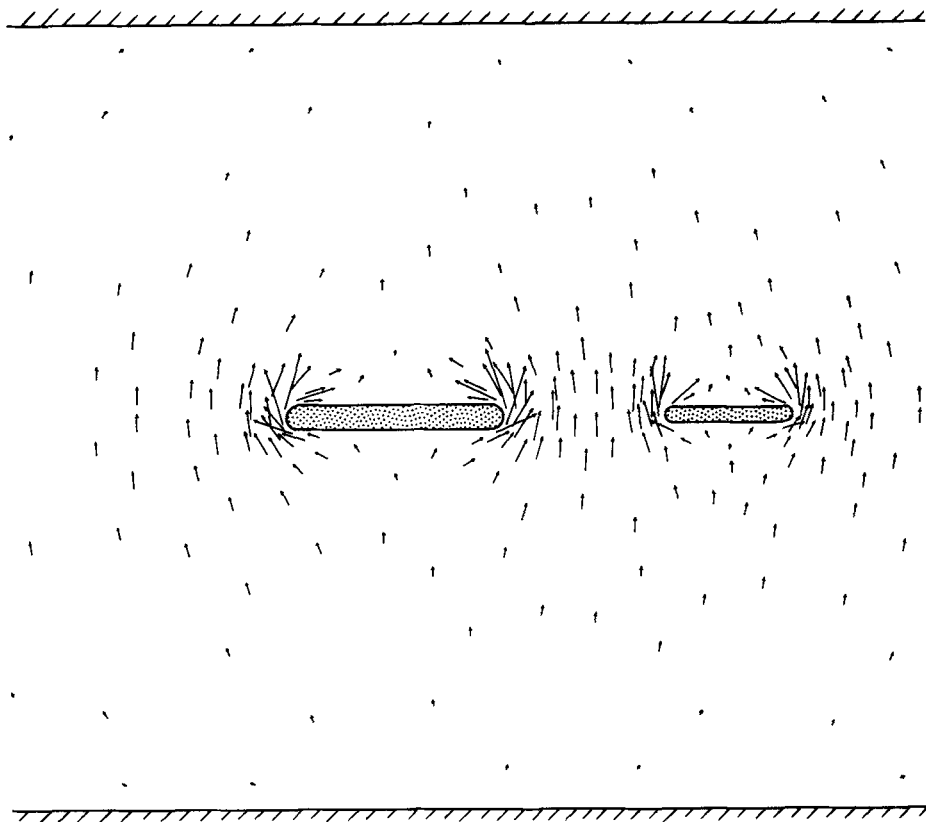The acoustic particle velocity directions corresponding to the pressure field of

FIGURE 8. Resonant acoustic particle velocities, corresponding to the simplest acoustic mode for two straight plates located in tandem in a duct at a spacing of $x/t = 6.25$ (50 mm), at the instant when the velocities are a maximum in the upwards direction; the lengths of the arrows indicate relative velocity magnitudes.

figure 7 are shown in figure 8. The velocity magnitudes vary harmonically; for half the sound cycle, the directional senses are opposite to those shown. Twice in each cycle the acoustic particle velocity is everywhere zero and twice the pressure is everywhere zero; these events are separated by a quarter-cycle, or 90°. In low-Mach-number flows, this phase relationship is only slightly different. In general, the acoustic particle velocities in the duct are directed across the flow. However, between the leading and trailing edges of each plate, the acoustic particle velocities reduce in magnitude and are approximately parallel to the flow direction.

4.2. *Observed resonance with a single plate*

As the flow velocity is increased from zero with the upstream plate (66.7 by 8 mm) installed alone, the frequency of the vortex shedding from the plate increases approximately linearly with flow velocity. When the shedding frequency is close to the Parker β-mode acoustic resonant frequency (684–691 Hz on figure 9) at a flow velocity of ≈ 21.4 m s^{-1}, the SPL generated by the flow at the acoustic resonant frequency is ≈ 124 dB (re 20 µPa) and the averaged spectrum of the hot-wire signal shows two spectral peaks, one at the sound frequency and the other close to the natural Strouhal value. This is shown in figure 9 by the existence of two vortex
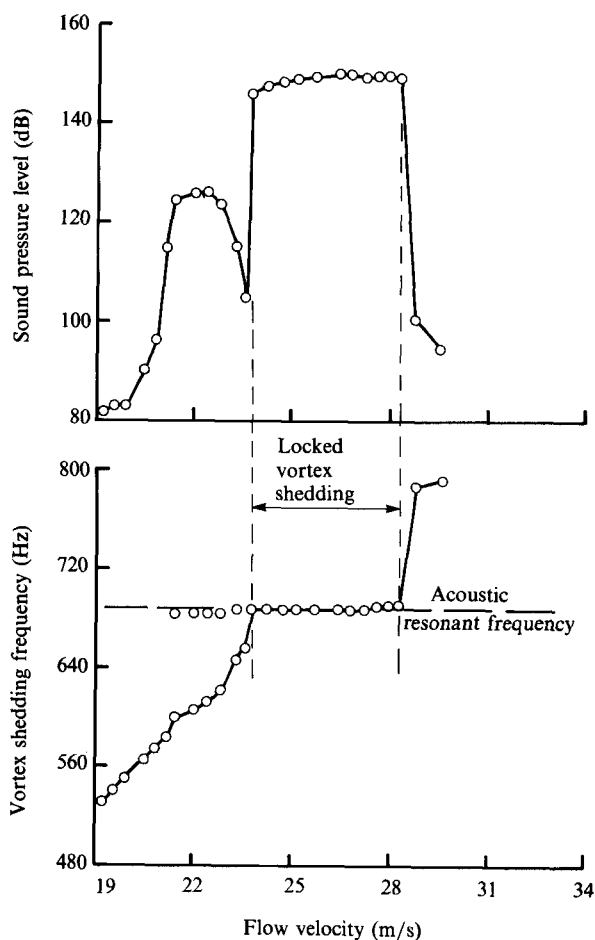
FIGURE 9. Variation of the vortex shedding frequency and the SPL (at the acoustic resonant frequency) with flow velocity for the upstream straight plate installed alone in the duct.

shedding frequencies at the same flow velocity and normally occurs when the resonant SPL is less than 140 dB and greater than 100 dB. As the flow velocity is increased up to 22 m s^{-1}, the SPL at the resonant frequency reaches 126 dB before reducing at flow velocities less than 24 m s^{-1}. At 24 m s^{-1}, loud resonant sound of $\approx$ 144 dB is generated and this occurs when the perturbations due to the sound field feed back onto the shear layers separating from the trailing edge of the plate and synchronizes the frequency of the vortex shedding with the resonant sound frequency. This phenomenon is known as 'lock-on', which manifests itself on the averaged spectrum of the hot-wire signal as a single marked peak at the acoustic resonant frequency. The frequency range over which vortex shedding is locked is shown on figure 9 where there is only one vortex shedding data point, at the acoustic resonant frequency, for a given flow velocity. It normally occurs when the SPL is greater than 140 dB.

With an increase in the flow velocity up to 26.4 m s^{-1}, the SPL at the probe microphone reaches $\approx$ 150 dB. On reaching 28.2 m s^{-1}, the SPL at the resonant frequency suddenly reduces, the vortex shedding unlocks from the resonant sound field and the vortex shedding frequency increases up to near the natural Strouhal
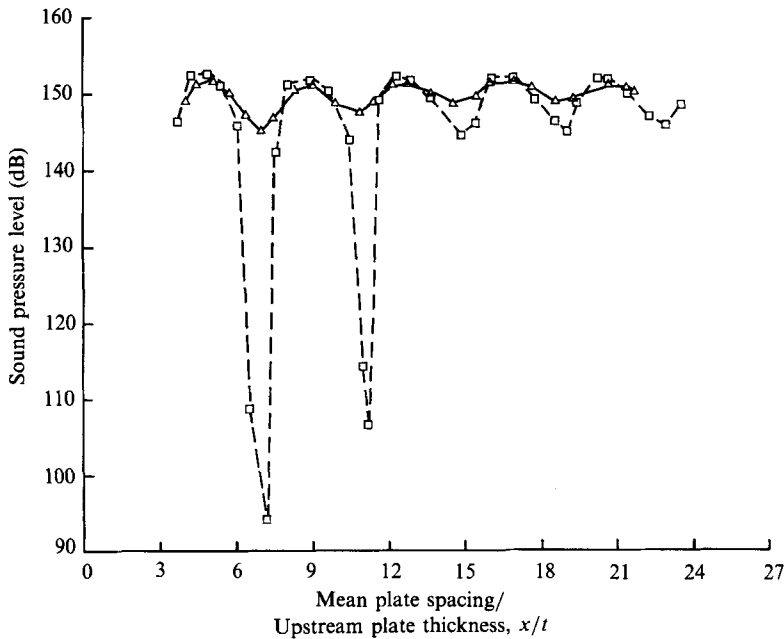
FIGURE 10. Variation of SPL (at the acoustic resonant frequency) with plate spacing at a flow velocity of 25.1 m s^{-1}: $-\square-$, straight downstream plate; $-\triangle-$, offset downstream plate.

value. This process is described in detail by Welsh et al. (1984) for a plate of shape similar to the upstream plate described in this paper.

4.3. Observed resonance with locked vortex shedding produced by two straight plates in tandem

As described above and shown in figure 9, at a flow velocity of 25.1 m s^{-1} with the upstream plate installed alone, loud resonant sound is generated and the vortex shedding frequency is locked to the sound frequency. When a downstream plate, with a chord of 40 mm and a thickness of 5 mm, is located in tandem with the upstream plate at the same flow velocity, the amplitude of the acoustic field is very dependent on the spacing between the two plates (figure 10). At a spacing of $x/t = 4.86$, the SPL is 153 dB, which is greater than that recorded with the upstream plate alone (150 dB). At a plate spacing of $x/t = 7.18$ the SPL, at the acoustic resonant frequency, reduces by 59 dB to a level of 94 dB; here, the vortex shedding is locked and its frequency reverts to the natural Strouhal value. The SPL continues to fluctuate as the plate spacing is increased up to $x/t = 23.5$ with the locations of successive maxima occurring regularly at intervals of $\Delta(x/t) \approx 3.75$. However, the amplitude of the fluctuation decreases with increasing plate spacing and, at spacings greater than $x/t = 12$, the vortex shedding frequency is always locked to the resonant sound frequency.

The photograph in figure 11 shows the flow of velocity 22.9 m s^{-1} around the two straight plates located at a spacing of $x/t = 3.75$ (30 mm) with locked vortex shedding. The acoustic particle velocities are a maximum in the upwards directional sense and the SPL at the acoustic resonant frequency recorded by the probe microphone is 152 dB. This photograph was obtained by exposing the same film at twenty different maxima of the acoustic particle velocity cycle (velocity upwards).
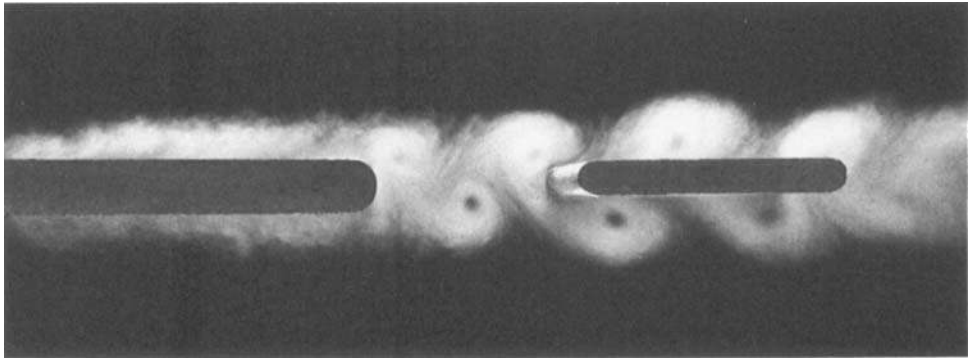
FIGURE 11. Photograph of the flow around the straight plates at a spacing of $x/t = 3.75$ (30 mm) at the instant in the sound cycle corresponding to maximum upwards acoustic particle velocity; upstream flow velocity $= 22.9$ m s^{-1}.
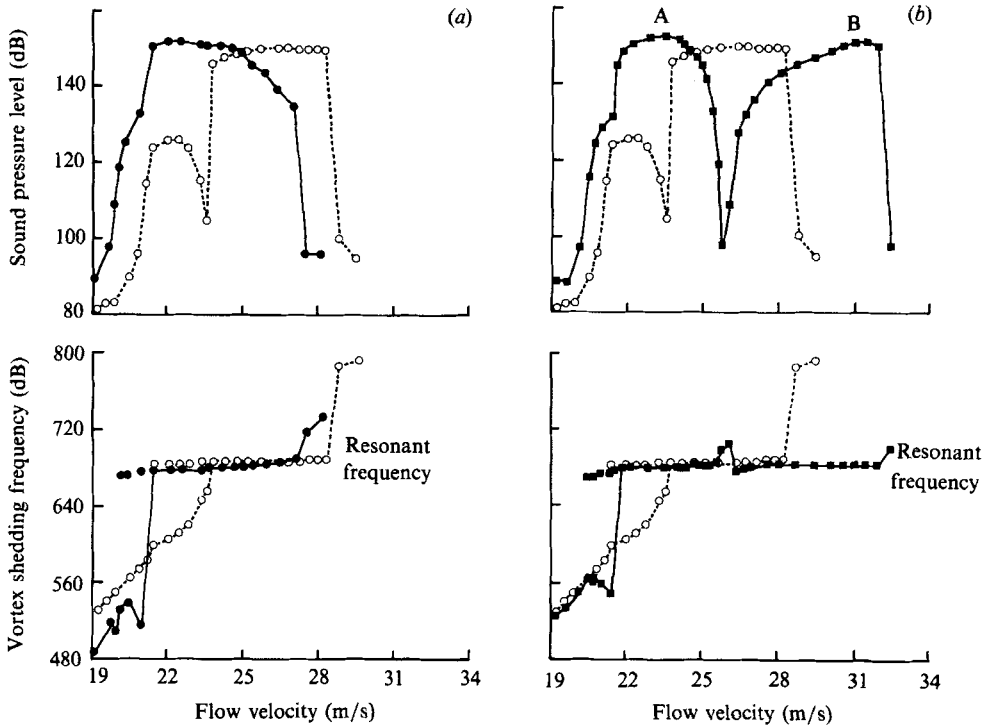

FIGURE 12. Variation of the SPL (at the acoustic resonant frequency) and vortex shedding frequency with flow velocity, for the upstream straight plate installed alone, and in tandem with a downstream straight plate at various spacings: $-\bigcirc-$, upstream plate installed alone; A, low velocity range with resonance; B, higher velocity range with resonance; (a) $-\bullet-$, $x/t = 3.75$; (b) $-\blacksquare-$, $x/t = 7.5$.

The superposition indicates the periodicity at which coherent large-scale vortex structures are shed into the wake.

More details of the influence of the downstream plate on the acoustic resonances generated for flow velocities ranging from 19.0 to 32.4 m s^{-1} are shown in figure 12. The data for the upstream plate installed alone, which were plotted in figure 9, are
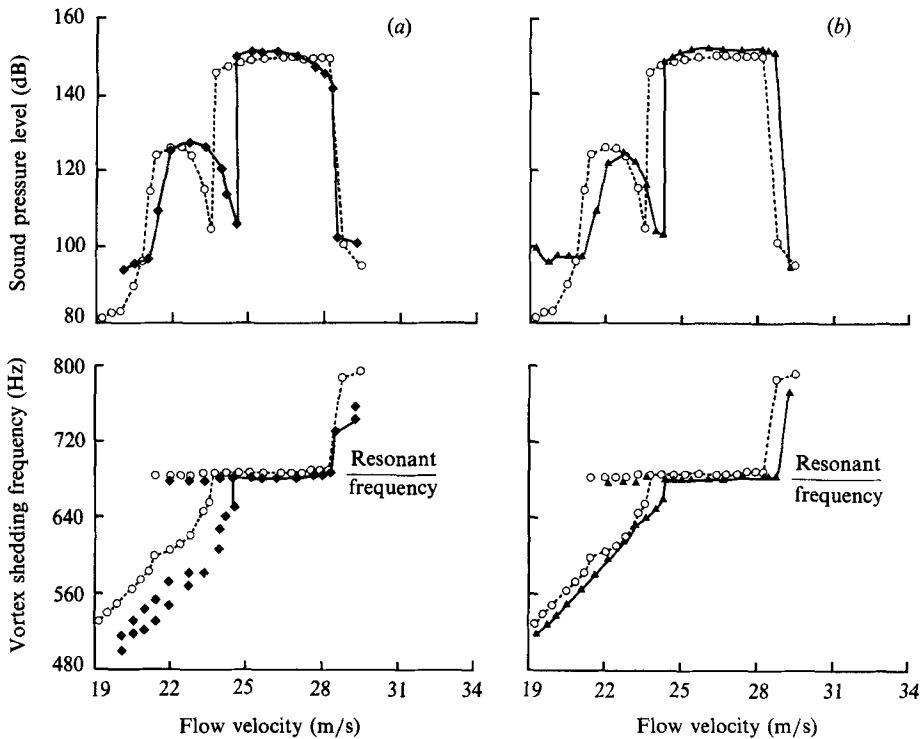
FIGURE 13. Variation of the SPL (at the acoustic resonant frequency) and vortex shedding frequency with flow velocity for the upstream plate installed alone, and for the upstream plate in tandem with a downstream offset plate at various mean spacings: O--O, upstream plate installed alone; (a) ◆-◆-, $x/t = 4.25$; (b) ▲-▲-, $x/t = 5.5$.

superimposed for comparison. For a spacing of $x/t = 3.75$ (figure 12a), loud resonant sound and locked vortex shedding are generated at flow velocities lower than those recorded for the upstream plate alone. Locked vortex shedding first occurs at a flow velocity of 21.4 m s^{-1} when the SPL reaches 150 dB.

When the flow velocity increases and approaches 27 m s^{-1} (figure 12a), the vortex shedding frequency remains locked to the resonant sound frequency, while the SPL gradually reduces to 134 dB. Locked shedding at an SPL below 140 dB is unusual, but can occur when the sound frequency is close to the natural Strouhal shedding frequency as observed here. If the flow exceeds 27 m s^{-1}, the loud resonant sound and locked vortex shedding cease, and vortex shedding at the Strouhal frequency resumes.

At spacings of $x/t = 5.0, 6.25$ and 7.5 (40, 50 and 60 mm), the last of which is shown in figure 12(b), loud resonant sound and locked vortex shedding occur over two discrete ranges of flow velocity (designated A and B) for each plate spacing. That is, the inclusion of the downstream plate leads to resonant sound being generated over a velocity range additional to the single range in the case of the upstream plate installed alone. Multiple ranges of locked vortex shedding were also obtained by Stoneman (1984) in an axial flow compressor test rig.

The maximum SPL for two plates is greater than the maximum value recorded with the upstream plate alone and, in the regions where the vortex shedding is not locked, the SPL at the resonant frequency reduces significantly. In general, the SPL
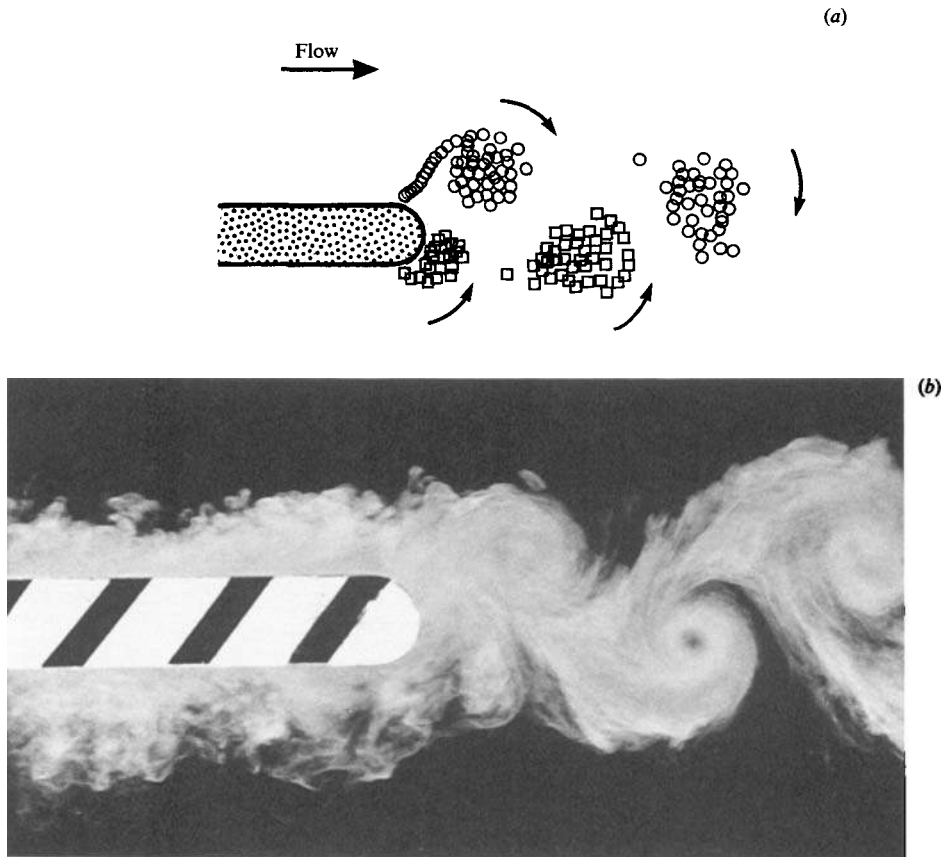
FIGURE 14. Comparison of (*a*) the vortex clouds in the predicted flow: ○, clockwise rotating vortices; □, counterclockwise rotating vortices, and (*b*) the vortex structures from a flash photograph of observed flow using smoke visualization (from Welsh *et al.* 1984) at the same phase of the acoustic cycle.

reached during locked vortex shedding over the lower velocity range A is lower than that recorded over the higher velocity range B; an exception occurs at a spacing of $x/t = 7.5$ (figure 12*b*).

Without loud resonant sound, the natural Strouhal vortex shedding frequencies (figure 12), vary slight with the proximity of the downstream plate. The closer the plates are together, the lower is the natural shedding frequency at the same flow velocity.

4.4. *Observed resonance with locked vortex shedding and an offset trailing plate*

Flow at a fixed velocity of 25 m s^{-1} was used to examine the different effects produced when the straight downstream plate was replaced by the offset plate described in §2. Increasing the plate spacing (figure 10) again causes the SPL to oscillate with peaks occurring at intervals of approximately $\Delta(x/t) = 3.75$. However, the maximum variation in the SPL is only 6 dB, which is much less than that recorded with the straight downstream plate installed (59 dB).

For different fixed locations of the offset plate, figure 13 shows the change in SPL and vortex shedding frequency with flow velocity. Data for the upstream plate
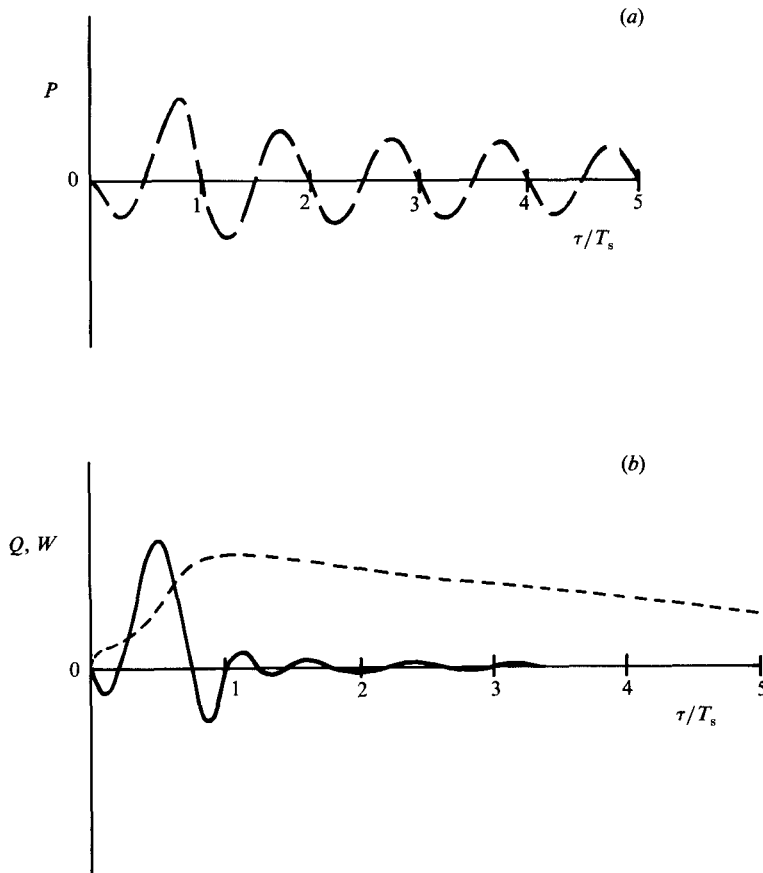
FIGURE 15. Predicted variation of (*a*) the instantaneous acoustic power output *P* and (*b*) the functions *W* and *Q* with time for a vortex cloud forming at time zero at the trailing edge of the upstream plate installed alone: —–––, *P*; -----, *Q*; ———, *W*. The *P*, *W* and *Q* units are arbitrary. T_s is the period of an acoustic cycle.

installed alone are included for comparison. The influence of the offset plate on changing the occurrence of resonance and locked vortex shedding, from that recorded with the upstream plate alone, is much less than that recorded with the straight downstream plate installed (figure 12). In particular, with locked vortex shedding and the offset downstream plate installed, the lower flow velocity range, A on figure 12, no longer exists. There is just one flow velocity range with locked vortex shedding and acoustic resonance, which is very similar to that observed for the upstream plate installed alone.

4.5. *Results from the mathematical model*

4.5.1. *Single-plate case*

In the discrete vortex model described in §3.2, the elemental vortices that are shed from the trailing edge of the upstream plate aggregate into clouds. When the transverse oscillating velocity field associated with the β-mode predicted by the finite-element solution to the Helmholtz equation (see §3.1) is incorporated via (3.8) in the vortex model of the flow around the single plate, the frequency with which these clouds are formed is found to be strictly locked to the sound frequency. During each
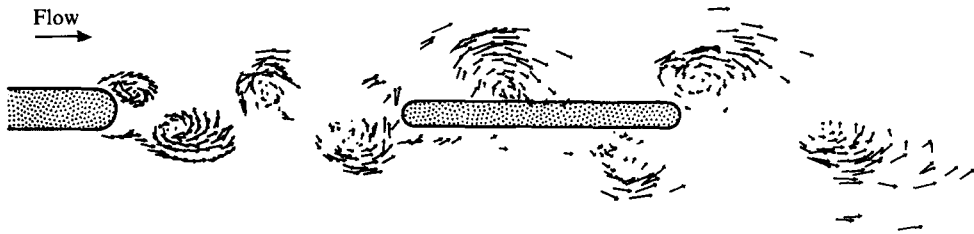
FIGURE 16. Predicted instantaneous velocity vectors associated with the elemental vortices in the tandem plate case with plate spacing $x/t = 5$. The arrows have origins at the centres of the elemental vortices and indicate the directions and relative magnitudes of the vortex velocities.
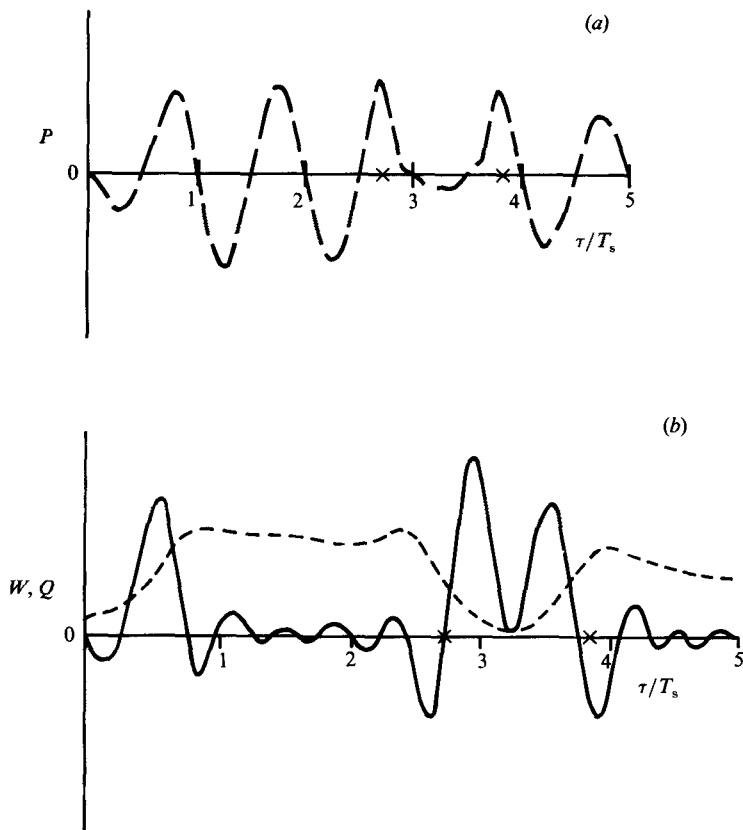

FIGURE 17. Predicted variation of (a) the instantaneous power output P and (b) the W and Q functions for a single vortex cloud during the first 5 acoustic cycles of its existence for the plate spacing $x/t = 8.1$: ————, P; - - - - -, Q; ———, W: ×, instants when the vortex cloud centre passes the leading and trailing edges of the downstream plate. The P, W and Q units are arbitrary. T_s is the period of an acoustic cycle.

sound cycle, new vortex clouds, of net opposite circulation, begin to form alternately from the upper and lower surfaces near the trailing edge of the plate. The phase of the acoustic cycle at which a new vortex cloud begins to form appears, from both experiment (Welsh *et al.* 1984) and the current predictions, to be when the acoustic particle velocity begins to augment the flow velocity near the separation point.
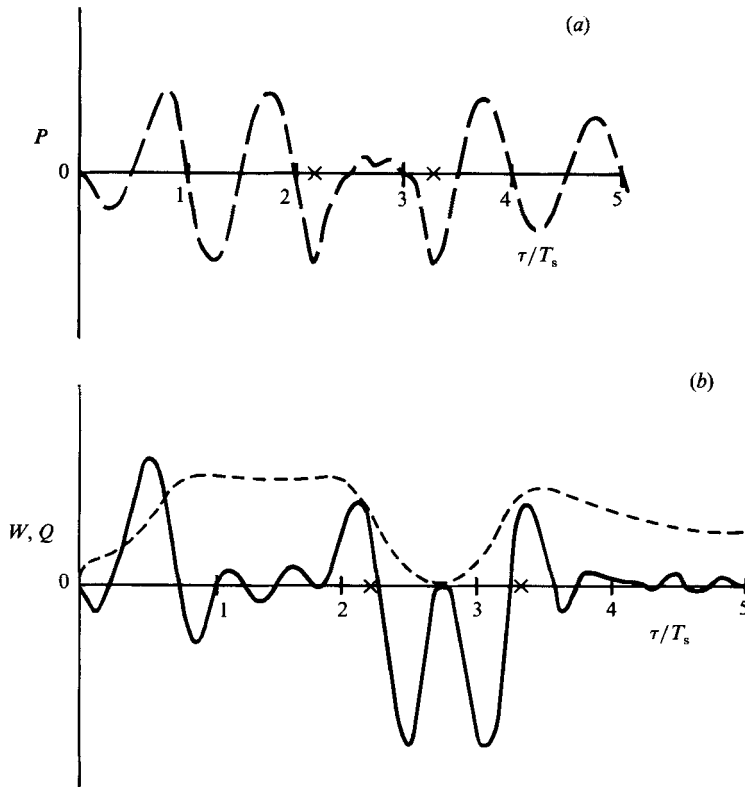
Figure 18. Predicted variation of (a) the instantaneous power output P and (b) the W and Q functions for a single vortex cloud during the first 5 acoustic cycles of its existence for the plate spacing $x/t = 6.3$: ————, P; ————, Q; ——, W; ×, instants when the vortex cloud centre passes the leading and trailing edges of the downstream plate. The P, W and Q units are arbitrary. T_s is the period of an acoustic cycle.

Figure 14 shows a comparison of the predicted flow and the flow observed by Welsh et al. (1984) at the same phase of shedding for the same Strouhal number.

From both the predicted and observed results, the vortex clouds, consisting of many smaller elemental vortices, retain their identities to a high degree as they are convected away from the vortex formation region at the trailing edge of the plate. It is possible therefore to follow the individual elemental vortices that comprise a particular vortex cloud. The instantaneous power output varies linearly with circulation according to (3.10). The time history of the instantaneous acoustic power output P of a vortex cloud can then be calculated from the sum of the outputs of the constituent elemental vortices. The very periodic nature of the vortex shedding process in the locked case results in near-identical time histories for different vortex clouds.

The acoustic power output predicted for a vortex cloud from its time of formation is shown in figure 15(a). Of special note is the significant imbalance between the power absorbed during the first acoustic half-cycle and the power generated during the second acoustic half-cycle. This imbalance, which was predicted by a more restricted mathematical model in Welsh et al. (1984), is more clearly seen in figure 15(b) showing the plots of the functions Q and W, defined in (3.12) and (3.14). Figure 15(b) indicates a net positive contribution to the energy integral in the trailing-edge
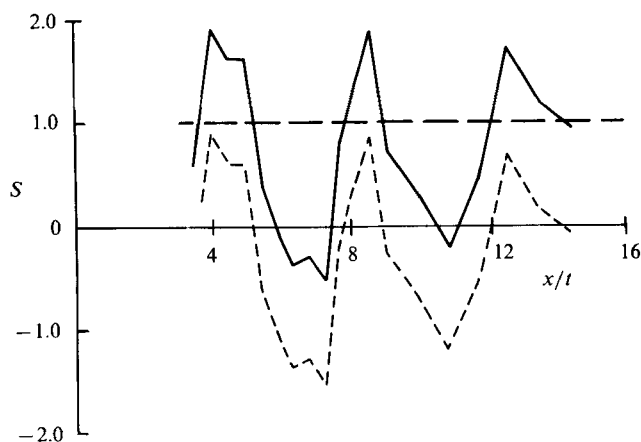
FIGURE 19. Variation with plate spacing x/t of the predicted net acoustic energy per cycle S generated by the wake for the tandem-plate case: ———, total net energy per cycle; – – – –, net energy per cycle generated by the source near the trailing edge of the upstream plate; - - - - -, net energy per acoustic cycle generated by the source near the downstream plate. The predicted energies are normalized to the value of the case of the upstream plate installed alone.

region of the single plate. Here, Q is fitted with a least-squares approximation before its derivative is used to calculate W. The function Q is zero at time zero when the vortex cloud begins to form and steadily increases over the first cycle as the vortex cloud grows and accelerates away from the plate. In subsequent cycles, Q decreases with time as the vortex has finished growing and there is an exponential decay in the acoustic particle velocity. The function W, which when integrated over time gives the total acoustic energy contributed by the vortex cloud, indicates the regions where net acoustic energy due to a vortex cloud is generated. Near the trailing edge of the plate, a significant positive peak is located which is not matched by negative peaks.

4.5.2. *Tandem-plate case with a straight downstream plate*

The introduction of a downstream plate into the wake of the upstream plate introduces an additional modification to the acoustic field, as described in §4.1. However, the acoustic field near the upstream plate for the plate spacings considered here is not substantially altered by the presence of the downstream plate. The predicted vortex shedding frequency is again found to lock to the acoustic frequency, as in the case of the single plate. A plot of the predicted velocities associated with the elemental vortices, showing the vortex clouds that constitute the wake for a plate spacing of $x/t = 5$, is illustrated in figure 16. The vortex clouds are convected virtually intact around the downstream plate, in line with the flow visualization shown in figure 11.

In figures 17 and 18, for two different plate separations $x/t = 8.1$ and 6.3, the instantaneous acoustic power P, together with the quantities Q and W derived in §3, are plotted for the passage of a single vortex cloud leaving the upstream plate and passing the downstream plate. Q, which is the amplitude of the power, has a magnitude that decays gradually except during the first cycle, where it increases from zero, and on passing the downstream plate, where it reduces nearly to zero for half a cycle. The resultant W, which is obtained from Q via (3.14), is shown in figures 17(*b*) and 18(*b*). Near the upstream plate, the values of W for the two plate spacings
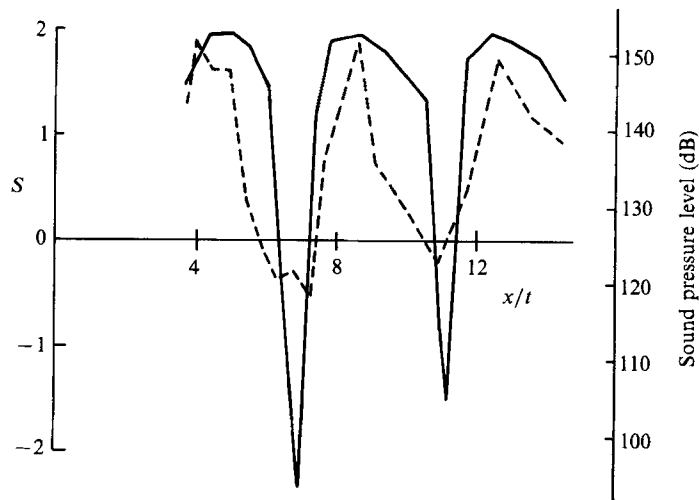
FIGURE 20. Variation of the measured SPL (at the acoustic resonant frequency and a flow of velocity of 25.1 m s^{-1}) and the predicted net acoustic energy per cycle S generated by the wake, for the tandem-plate case with a straight downstream plate: ——, measured SPL; -----, predicted acoustic energy output per cycle. The predicted energy is normalized to the value of the case of the upstream plate installed alone.

are similar to those obtained for the single-plate case (figure 15b). However, further downstream, the values of W for these two plate spacings differ markedly from each other and from the single-plate case. Near the downstream plate, the net value of W is positive or negative depending on the plate spacing. The reason for the alternating values of W will be discussed later (§5.2).

Comparing the plots of W in figures 15(b), 17(b) and 18(b), it can be seen that there are two distinct regions in which W is significantly non-zero; these regions occur near the trailing edge of the upstream plate and in the region of the downstream plate. For the purposes of estimating the relative contributions from each of these regions, W can effectively be decoupled into contributions from the upstream-plate region, $x/t \leqslant 1.5$, and the downstream-plate region, $x/t > 1.5$. The predicted net acoustic energy output per cycle S of a wake of vortices is calculated from the integration of the function W and summed over the wake. S is shown for different plates spacings in figure 19, which also shows the individual contributions to the energy S from the upstream- and downstream-plate regions.

The predicted net acoustic energy produced by the wake per sound cycle (figure 19) and the observed resonant SPL for a straight downstream plate (figure 10) are shown as a function of the non-dimensional plate spacing in figure 20. Clearly maximum and minimum predicted acoustic energy output corresponds with measured maximum and minimum SPL.

4.5.3. Tandem-plate case with an offset downstream plate

A prediction of the acoustic sources of an offset plate can be made by averaging the values of W shown in figures 17 and 18. Because the degree to which the plate is offset is much smaller than the acoustic wavelength and the resonant duct frequency is independent of whether a straight or offset plate is installed as the downstream plate, the resonant sound and flow fields may be assumed two-dimensional across each half of the offset plate. Each half of the plate has a different spacing, with values of
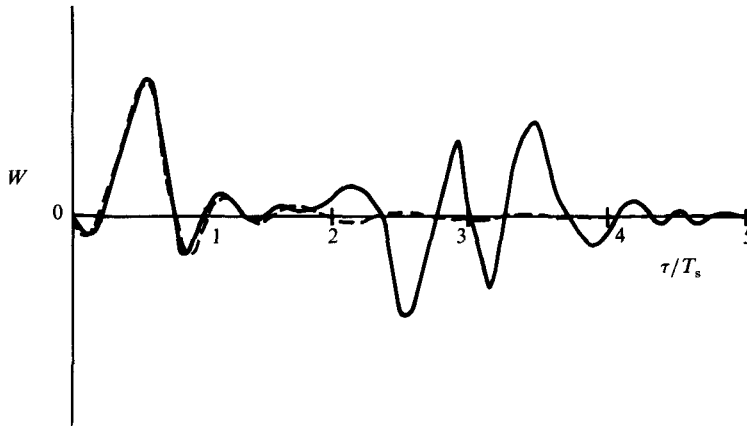
FIGURE 21. Predicted variation with time of the W functions (arbitrary units) for the upstream plate installed alone and for the upstream plate installed with an offset downstream plate: ——, offset downstream plate and upstream plate with mean spacing $x/t = 7.2$; -----, upstream plate installed alone. T_s is the period of an acoustic cycle.

$x/t = 6.3$ and 8.1 or mean $x/t = 7.2$; in figure 21, the predicted results of figures 17 and 18 are averaged spanwise and the resultant W compared with the results for a single plate. The main difference is the occurrence of positive and negative peaks, of approximately equal magnitude, in the downstream-plate region which are not predicted in the comparable region for a single plate.

5. Discussion of results

5.1. *Stable acoustic resonance with a single plate in a duct*

The results from the mathematical model described here (figure 15) show that as the flow passes the semicircular trailing edge of a plate located in a duct, an acoustic source is created by the vortex clouds forming at the resonant acoustic frequency (locked vortex shedding). The net contribution of the acoustic power (3.9) from a single vortex cloud as it passes through the sound field is dominated by the events in the first cycle of vortex growth, as shown in figure 15 (*a*). This is the period when Q (§§3.3, 4.5.1) changes rapidly, mainly due to the change in circulation of the growing vortex. Quantitatively, these effects are clearer in figure 15 (*b*) showing W, the integral of which over the lifetime of the vortex cloud, like that of P, corresponds to the net energy transferred from the flow to the sound field. The large positive peak in W near the trailing edge indicates that, during the sound cycle in which the vortex cloud forms, the net acoustic energy generated by the cloud is positive. This leads to the vortex formation region being an acoustic source. After the first sound cycle of existence of a vortex cloud, there is negligible net acoustic energy generated (Welsh *et al.* 1984).

5.2. *Acoustic resonance with locked vortex shedding and two straight plates in tandem*

When, at a constant flow velocity of 25.1 m s^{-1}, the spacing between two straight plates located in tandem is progressively increased from $x/t = 3.75$, the SPL at the resonant frequency fluctuates as shown in figure 10. This fluctuation is similar to that described by Johnson & Loehrke (1984) for two plates with thick trailing edges located in tandem in an open jet of high Reynolds number; they attributed the effect

to multiple sound sources near the plates. However, in their case, there appeared to be negligible effect of the sound on the vortex shedding process. In this study, the SPL obtained for the duct resonance is much higher than that obtained by Johnson & Loehrke (1984) in an open jet; at this higher SPL, the sound feeds back onto the flow and synchronizes the vortex shedding from the upstream plate. Nevertheless, multiple sources are predicted in the flow by the vortex model even though the details of the sources may be different from those proposed by Johnson & Loehrke (1984). In the following discussion, one of the sources is shown to be located near the upstream plate and is similar to that found in §5.1 with a single plate. The other important region is near the downstream plate and it may be a source or sink depending on plate spacing.

The effect of the synchronization of the vortex shedding at the trailing edge of the upstream plate is that one vortex is shed each acoustic cycle from near each of the upper and lower surfaces of the plate. The phase of this shedding is fixed and does not vary with plate spacing. The details of the acoustic power output near this trailing edge are therefore independent of the location of a downstream plate. There is a large positive peak in W near this trailing edge whenever the vortex shedding is locked, producing an acoustic source. This peak in W is seen for particular plate spacings in figure 17(b) and 18(b) (as well as in the single-plate case, figure 15b). Figure 19 shows that the trailing-edge region of the upstream plate is a net acoustic source of constant strength for all plate spacings; its strength is equal to the value for a single plate installed alone.

The predicted net acoustic energy per cycle S contributed by the vortex street in the downstream-plate region fluctuates with plate spacing, as shown in figure 19. In particular, for two different plate spacings, figure 17(b) and 18(b) show that W can change from having predominantly positive peaks to predominantly negative peaks near the downstream plate. That is, this region of the flow is either an acoustic source or a sink depending on the plate spacing.

The variation of the downstream plate source with spacing can be understood by considering the simplified case discussed in §3.3. In figures 3 and 5, the passage of the vortex past a plate (such as the downstream plate used in these experiments) results in the generation of net positive acoustic energy for a particular choice of h. However, if the vortex had arrived at the plate half an acoustic cycle later, h in (3.14) is increased by 180° and the net contributed acoustic energy according to (3.14) has the same magnitude but is negative. That is, the region around the plate becomes an acoustic sink owing to the later arrival of the vortex. In the tandem-plate case, the shedding of vortices from the upstream plate always occurs at the same instant in the acoustic cycle for locked vortex shedding. Consequently, for constant flow velocity, the time of arrival of the vortex at the downstream plate, and therefore the value of h, depends only on the plate spacing. The distance travelled by a vortex in a sound cycle is the distance between adjacent vortices in the same row. During the time a vortex travels this distance, h increases by 360°. Therefore, the period of the spatial oscillation seen in figure 10, which is about 30 mm or 3.75 plate thickness, should be similar to the observed vortex spacing, and this is verified in figure 11.

The effects of the two source regions described are additive, and their combined effect produces a variation of S with plate spacing as shown in figure 20; the observed SPL is plotted for comparison. Although the two scales are different (the SPL is logarithmic), the spatial periodicity is clearly very similar. Peaks in the SPL correspond to peaks in the predicted rate of generation of acoustic energy. This provides confidence in the concept of multiple sources being present in the flow.

The number of source regions to which the sound is attributed is somewhat arbitrary; in particular it might be useful to consider the leading- and trailing-edge regions of the downstream plate separately. For the chord used here, these subregions acted together as sources or sinks, but if the chord were longer or the Strouhal number different, there might be contrasting behaviour which should be taken into account.

5.3. *Acoustic resonance with one straight plate and an offset plate located downstream in tandem*

The design of the offset plate was motivated by the explanation of the tandem-plate observations given above. Two equally effective source regions placed so that vortices always pass at opposite phases of the sound cycle should cancel each other. This can be achieved by offsetting half of the downstream plate (figure 1) in the flow direction by approximately half the distance between adjacent vortices in the same row of the vortex street. Since the vortices are shed simultaneously across the entire span of the upstream plate, one half of each vortex tube will reach the offset plate half an acoustic cycle sooner than does the other half of the same vortex tube. Consequently, following the description of acoustic sources in §§3.3, 4.5 and 5.2, the acoustic energy generated near one half of the offset plate will be equal in magnitude but opposite in sign to the acoustic energy generated near the other half of the offset plate. This is illustrated in figure 21 where W, averaged spanwise, for an offset plate case has a net time integral similar to that for the upstream plate installed alone.

The data in figures 10 and 13 show that, independent of the plate spacing, the introduction of the offset plate has little effect on the resonances and locked vortex shedding observed with the upstream plate alone. The clear implication is that the flow around the offset plate does not contribute a net supply of acoustic energy, as shown by the mathematical model results in figure 21.

5.4. *Possible applications to the suppression of acoustic resonances in industrial equipment*

Abd-Rabbo & Weaver (1986) have provided irrefutable evidence of discrete vortex shedding in a staggered tube array. It is therefore reasonable to assume that vortex shedding is the source of acoustic resonances in multitube row or multiblade row equipment. Two kinds of remedies for resonance in such equipment are therefore suggested by this work. Bearing in mind the phase dependence of acoustic sources that are located downstream of where vortices are shed into the flow, the tube or blade associated with this source can be moved to locations where vortices passing around the tube or blade will absorb sound. If this acoustic source region can absorb more acoustic energy than that being generated by other sources, then there is no net supply of acoustic energy and resonant sound ceases. This approach to the suppression of acoustic resonances must be used cautiously because a particular spacing will give the necessary phase relationship to suppress resonance only at a particular limited range of flow velocities. At other flow velocities the same spacing would augment resonance; a different spacing would be necessary for their suppression.

The second remedy, which is less sensitive to flow velocity variation, is to redesign the tubing or blades associated with acoustic sources in the flow downstream of the point where vortices are shed, so that the associated acoustic source makes no net contribution to the supply of acoustic energy to sustain resonance. This technique is useful for suppressing resonances that occur only when a particular blade or tube row

is installed in tandem to an existing row, but are not excited when the tandem row is absent. The results reported here, using the offset modification to the downstream plate, show that it is possible to adjust the geometry so that there is no net acoustic energy generated by the flow around the tandem row.

The offset modification may not be practical, but the results reported in this paper support the idea of using acoustic sources and sinks to cancel each other and suggest there may be other ways to ensure that the flow around tubes or blading will not be net acoustic source regions. It is possible that the necessary spread of phase relationships between the acoustic field and the vortex motions, which lead to cancellation, could be obtained by slanting the tubes or blades in the flow direction by prescribed amounts. Therefore, with the new operating procedures employed with axial compressors, it is realistic to conceive a blade geometry that maintains the necessary phase relationship between the separated flows and possible acoustic fields to ensure acoustic resonances are not generated.

6. Conclusions

Flow past a rounded plate placed horizontally at the centre of a duct may, within a certain range of velocities, induce a β-mode acoustic resonance with locked vortex shedding. Placing a second plate downstream in tandem with it can suppress resonance and locked vortex shedding at specific flow velocities. At other velocities, resonances occur that are not observed with the upstream plate alone.

The effect of the downstream plate depends on its distance from the upstream plate. The increased propensity to resonate due to the downstream plate can be countered by bisecting this plate in the spanwise direction and rejoining the two halves offset in the flow direction by a distance equal to half the spacing between adjacent vortices in a row of the vortex street.

These observations can be explained using Howe's (1984) theory of aerodynamic sound and taking account of the changes to the resonant acoustic field caused by the presence of the downstream plate. The explanation is consistent with the presence of multiple sound sources, as postulated by Johnson & Loerhke (1984).

When vortical flow passes around tubing in heat exchangers or blades in axial flow compressors, the present results suggest that the flow-induced loud acoustic resonances can be suppressed by either appropriate axial spacing of the rows or by varying the dimensions of the bodies so that any region that might act as an acoustic source is countered by a sink somewhere else.

The discrete vortex method, using surface vorticity to specify the boundary conditions, can be coupled with solutions of the Helmholtz equation and Howe's (1984) theory of aerodynamic sound to satisfactorily predict those regions in the flow that act as acoustic sources and sinks during resonance with two plates located in tandem in a duct. It should be possible to extend this technique to include additional rows and geometries.

REFERENCES

ABD-RABBO, A. & WEAVER, D. S. 1986 A flow visualization study of flow development in a staggered tube array. *J. Sound Vib.* **106**, 241–256.

ARCHIBALD, F. S. 1975 Self-excitation of acoustic resonances by vortex shedding. *J. Sound Vib.* **38**, 81–103.

BATCHELOR, G. K. & TOWNSEND, A. A. 1945 Singing corner vanes: a note on a peculiar double resonant sustained oscillation occurring in a wind tunnel. *CSIR, Division of Aerodynamics Note* 62.

BLEVINS, R. D. 1985 The effect of sound on vortex shedding from cylinders. *J. Fluid Mech.* **61**, 217–237.

BYRNE, K. P. 1983 The use of porous baffles to control acoustic vibrations in crossflow tubular heat exchangers. *Trans. ASME* C *J. Heat Transfer* **105**, 751–758.

CHANG, C. S. & YEH, Y.-G. 1981 A model for the analysis of air heater vibrations. *ASME Paper no. 81-DET-*34.

CHEN, Y. N. 1968 Flow-induced vibration and noise in tube-bank heat exchangers due to von Kármán streets. *Trans. ASME* B *J. Engng Indust.* **90**, 134–146.

CHEN, Y. N. 1972 Fluctuating lift forces of Kármán vortex sheets on circular cylinders and in tube bundles. *Trans. ASME* B *J. Engng Indust.* **99**, 623–628.

COWELL, T. A. & DAVENPORT, C. J. 1984 Acoustic resonance in air cooled heat exchangers. *First UK Natl Conf. on Heat Transfer, The Institution of Chemical Engineers Symp., Series No.* 86.

CRIGHTON, D. G. 1981 Acoustics as a branch of fluid mechanics. *J. Fluid Mech.* **106**, 261–298.

CUMPSTY, N. A. & WHITEHEAD, D. S. 1971 The excitation of acoustic resonances by vortex shedding. *J. Sound Vib.* **18**, 353–369.

FITZPATRICK, J. A. 1985 The prediction of flow-induced noise in heat exchanger tube arrays. *J. Sound Vib.* **99**, 425–435.

FITZPATRICK J. A. & DONALDSON, I. S. 1977 A preliminary study of flow and acoustic phenomena in tube banks. *Trans. ASME* I *J. Fluids Engng* **99**, 681–686.

HOWE, M. S. 1984 On the absorption of sound by turbulence. *IMA J. Appl. Maths* **32**, 187–209.

JOHNSON, C. O. & LOEHRKE, R. I. 1984 An experimental investigation of wake edge tones. *AIAA J.* **22**, 1249–1253.

KIYA, M., SASAKI, K. & ARIE, M. 1982 Discrete-vortex simulation of a turbulent separation bubble. *J. Fluid Mech.* **120**, 219–244.

LEWIS, R. I. 1981 Surface vorticity modelling of separated flows from two-dimensional bluff bodies of arbitrary shape. *J. Mech. Engng Sci.* **23**, 1–12.

MORTON, B. R. 1984 The generation and decay of vorticity. *Geophys. Astrophys. Fluid Dyn.* **86**, 277–308.

PARKER, R. 1966 Resonance effects in wake shedding from parallel plates: experimental observations. *J. Sound Vib.* **4**, 62–72.

PARKER, R. 1967a Resonance effects in wake shedding from parallel plates: calculation of resonant frequencies. *J. Sound Vib.* **5**, 330–343.

PARKER, R. 1967b Resonance effects in wake shedding from compressor blading. *J. Sound Vib.* **6**, 302–309.

PARKER, R. 1968 An investigation of acoustic resonance effects in an axial compressor stage. *J. Sound Vib.* **8**, 281–297.

PARKER, R. 1969 Discrete frequency noise generation due to fluid flow over blades, supporting spokes and similar bodies. *ASME 69-WA/GT-*13.

PARKER, R. & PRYCE, D. 1974 Wake excited resonances in an annular cascade: an experimental investigation. *J. Sound Vib.* **34**, 247–261.

PARKER, R. & STONEMAN, S. A. T. 1984 Acoustically excited vibration of compressor blades. *I. Mech. E. (UK) Third Intl Conf. on Vibrations in Rotating Machinery.* York, UK.

PARKER, R. & STONEMAN, S. A. T. 1985 An experimental investigation of the generation and

consequences of acoustic waves in an axial flow compressor: large axial spacings between blade rows. *J. Sound Vib.* **99**, 169–182.

PARKER, R., STONEMAN, S. A. T. & CARR, M. 1984 Excitation of blade vibration by flow induced acoustic resonances in axial flow compressors. *Unsteady Aerodynamics of Turbomachines and Propellers.* Jesus College, Cambridge.

ROCKWELL, D. 1982 Oscillations of impinging shear layers. *Invited lecture, 20th Aerospace Sciences Meeting, AIAA-82-0047,*

ROCKWELL, D. & NAUDASCHER, E. 1979 Self-sustained oscillations of impinging free shear layers. *Ann. Rev. Fluid Mech.* **11**, 67–94.

STOKES, A. N. & WELSH, M. C. 1986 Flow-resonant sound interaction in a duct containing a plate. Part II. Square leading edge. *J. Sound Vib.* **104**, 55–73.

STONEMAN, S. A. T. 1984 An experimental investigation of flow excited acoustic fields in an axial flow compressor. Ph.D. thesis, University College of Swansea.

WELSH, M. C. & GIBSON, D. C. 1979 Interaction of induced sound with flow past a square leading edge plate in a duct. *J. Sound Vib.* **67**, 501–511.

WELSH, M. C. & STOKES, A. N. 1986. Transient vortex modelling of flow induced acoustic resonances near cavities or obstructions in ducts. In *Proc. IUTAM Symp. on Aero and Hydroacoustics, Lyons,* pp. 499–505. Springer.

WELSH, M. C., STOKES, A. N. & PARKER, R. 1984 Flow-resonant sound interaction in a duct containing a plate. Part I. Semicircular leading edge. *J. Sound Vib.* **95**, 305–323.

ZDRAVKOVICH, M. M. & NUTTALL, J. A. 1974 On the elimination of aerodynamic noise in a staggered tube bank. *J. Sound Vib.* **34**, 173–177.